

Cyclic Behavior of DuraFuse Frames Moment Connections

PAUL W. RICHARDS

ABSTRACT

Most special moment frames (SMF) rely on beam yielding to reach drifts of 0.04 rad and beyond. In contrast, DuraFuse Frames (DFF) incorporate a fuse plate that acts as the yielding element. Nine full-scale DFF specimens were tested using AISC 341 (2016b), *Seismic Provisions for Structural Buildings*, Chapter K, to prequalify the DFF connection for use in SMF and inclusion in AISC 358 (2016a), *Prequalified Connections for Special and Intermediate Steel Moment Frames for Seismic Applications*. Eight specimens were tested with the standard protocol and exceeded the qualification criteria. The other specimen completed a custom protocol representing three maximum considered earthquakes (MCE) in sequence. The experiments demonstrated that the stiffness of the DFF connection is sufficient to classify the connection as fully restrained (FR).

Keywords: special moment frame, replaceable fuse, prequalified moment connection, experimental testing, DuraFuse, fully restrained connection.

INTRODUCTION

Steel special moment frames (SMF) are commonly used to resist earthquake effects in high seismic areas. Because SMF are designed with $R = 8$ (ASCE, 2016), they are expected to operate well in the inelastic range during severe earthquakes. AISC 341, *Seismic Provisions for Structural Steel Buildings*, hereafter referred to as AISC 341 (AISC, 2016b), Section E3.6b, specifies that SMF connections must demonstrate stable performance for drifts up to 0.04 rad.

Most SMF connections rely on beam yielding to provide some or all of the inelastic rotation required to accommodate these large-story drifts. Prequalified connections like the welded unreinforced flange-welded web (WUF-W) and reduced beam section (RBS) rely exclusively on beam yielding, while other connections, like the bolted flange plate (BFP) or double tee, rely on a combination of bolt slip and beam yielding (AISC, 2016b).

There are some drawbacks to relying on beam plastic hinges to achieve ductile SMF. Strict width-to-thickness ratios have to be imposed on the beams, limiting the shapes that can be used (AISC 341, Section D1.1b). Extra lateral bracing is required to keep the beams stable after plastic hinges form (AISC 341, Section D1.2). The portions of the beams subject to inelastic straining need to be designated as protected zones (AISC 341, Section E3.5c). After an earthquake, residual drifts may be locked into the frame

by deformed beams. A final drawback of relying on beam plastic hinges is that beam ends may need to be cut out and replaced after a severe earthquake, a challenging proposition that may be economically unfeasible.

DuraFuse Frames (DFF) take a different approach to achieving SMF ductility. Rather than having the beam form a plastic hinge, DFF connections incorporate a fuse plate that acts as the yielding element (UES, 2020).

Figure 1 shows one-sided DFF connections for I-shaped or HSS/box columns. Two-sided and biaxial DFF connections (not shown in Figure 1) are also permitted. For I-shaped columns, the column has cover plates on each side that are fillet welded to the column flanges, as shown in Figure 1(a). For box or HSS columns, the sides of the column may function as the cover plates, as shown in Figure 1(c). Four external continuity plates that extend past the face of the column are fillet welded to the column cover plates or side. The column has a shear tab, with horizontal slotted holes, that is fillet welded to the column face. The beam web, with standard holes, is attached to the shear tab with pretensioned bolts. The beam flanges are attached to the external continuity plates via top plates (top flange) and a fuse plate (bottom flange) (Figure 1). The fuse plate is proportioned such that certain regions of the plate experience shear yielding when the connection is subjected to severe earthquake loading [Figure 1(b)]. The fuse plate is bolted so that it could be removed and replaced following a severe earthquake. The top plates are intended to experience minimal yielding, such that they would not require repair following a severe earthquake. The various plates in the connection are proportioned such that the beam remains essentially elastic.

Several experimental studies have been performed to investigate the behavior of DFF connections subjected to

Paul W. Richards, Vice President of Research and Development, DuraFuse Frames, West Jordan, Utah. Email: paul.richards@durafuseframes.com

cyclic loads. Richards and Oh (2019) performed testing on reduced-scale DFF specimens that demonstrated good potential for the system. Richards (2019, 2021) reported other series of tests with full-scale DFF connections.

Additional testing was performed at the University of California–San Diego (UCSD) to prequalify the DFF connection for use in SMF (Reynolds and Uang, 2019a, 2019b). This paper presents results from nine full-scale DFF specimens that were tested at UCSD. The experiments will be described, and the results will be discussed in the context of AISC 341 criteria for SMF connections.

EXPERIMENTAL TESTING

Test Setup

The overall test setup and specimen geometry are shown in Figure 2. The specimens represented SMF subassemblies with one beam framing into the column (strong axis). The specimens were tested with the column vertical and the beam cantilevering out. To simulate inflection points, the ends of the specimen column were mounted on short sections of W14×257 positioned to experience weak-axis bending. For all specimens, the distance between column supports was 16 ft. For Series E, F, and G, the distance from the column centerline to the actuator line of action was 15.5 ft, while for Series H the distance was 20.5 ft [Figure 2(a)]. A corbel was bolted to the “free” end of the beam and attached to one end of a servo-controlled actuator. The other end of the actuator was mounted to the strong floor. Out-of-plane restraint was provided at the actuator location on both sides of the corbel [Figure 2(b)]. No lateral restraint was provided near the connection or at any other location along the length of the beam.

Connection Details

Four series of tests were performed (E, F, G, H), each with unique beam and column sizes. Table 1 provides beam size, column size, bolt size, and plate thicknesses for each series. Two tests were performed in the E, F, and G series, and three tests were performed in the H series, resulting in a total of nine tests (Table 1).

For each series, the beam size, column size, and connection plate thicknesses were constant (Table 1). Beam sizes ranged from W21 to W40, and beam weight ranged from 50 to 232 lb/ft. Wide-flange column sizes ranged from W14 to W36, and the box column for the H series was 24 in. deep. Fuse plate thicknesses ranged from 0.625 to 1.75 in., and cover plate thicknesses ranged from 0.375 to 0.875 in.

A variety of considerations influenced the beam sizes used in the study. The W36×232 was the strongest W36 beam that could be tested using the equipment/test setup available at the time without the beam length becoming excessive relative to common practice. The W40×167 beam was the strongest W40 beam that could be tested at the time with a 15.5-ft half-span length. The W36×232 and W40×167 had different flange widths that influenced the fuse plate geometry, so both were of interest. The W30×99 had a flange width-to-thickness ratio beyond λ_{pd} , to investigate relaxed width-to-thickness requirements. The W21×50, with a 15.5-ft unbraced length, was included to investigate relaxed lateral bracing requirements (this beam usually requires lateral bracing every 5.4 ft, per AISC 341, Section D1.2b). The four beam sizes used for the UCSD testing complimented beam sizes that had been used in previous DFF studies (W36×150, W33×152, W27×84, W14×38) (Richards, 2019; Richards, 2021; Richards and Oh, 2019).

The columns were selected to match the beam strengths, investigate torsional issues, and prequalify DFF

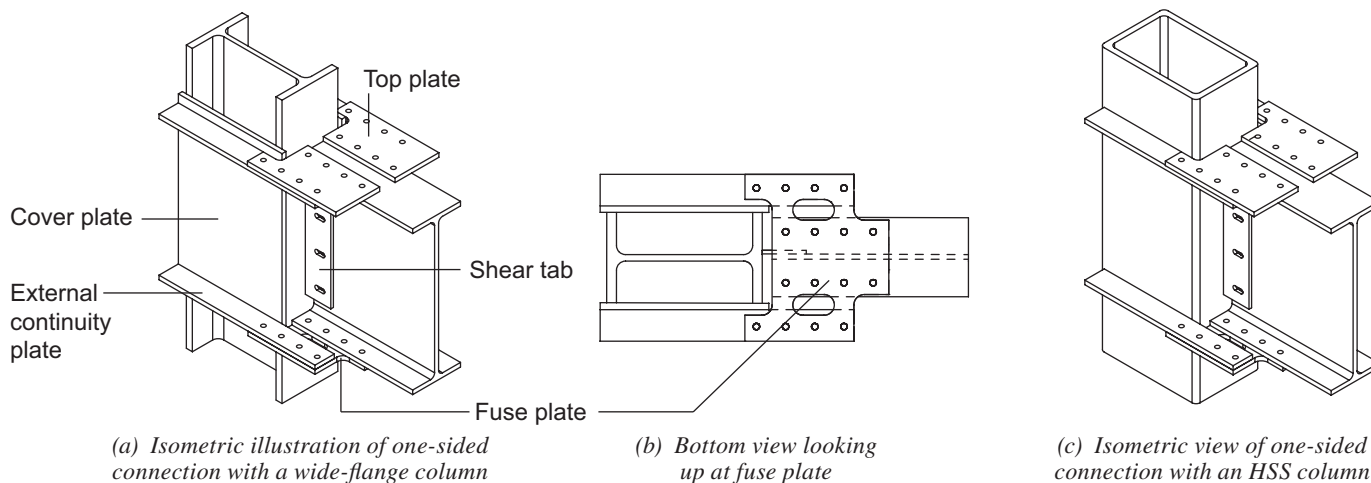
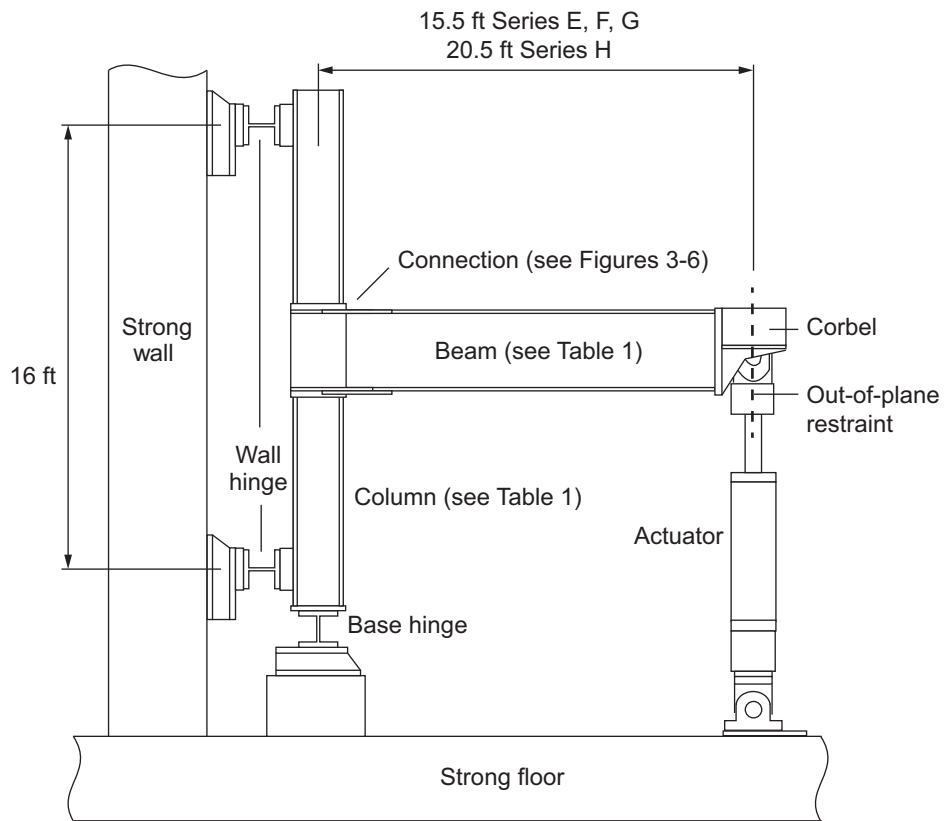


Fig. 1. DuraFuse Frames connection for SMF.



(a) Schematic with dimensions



(b) Installed specimen (G1.1) and out-of-plane restraint at actuator

Fig. 2. Experiment test setup.

Table 1. Member, Plate, and Bolt Sizes

Series	Specimens	Beam	Column	Fuse Thickness (in.)	Cover Plate Thickness (in.)	Bolt Size (in.)	Bolt Grade (ASTM F3125)
E	E1.1	W30×99	W21×132	0.75	0.625	1	F2280
	E1.2						
F	F1.1	W40×167	W36×231	1.25	0.875	1.125	F2280
	F1.2						
G	G1.1	W21×50	W14×68	0.625	0.375	0.875	F1852
	G1.2						
H	H1.1	W36×232	BOX24×17½×1¾	1.75	1.75 ^a	1.25	A490
	H1.2						
	H1.3						

^a The sides of the box column functioned as the cover plates for the H series.

connections for HSS/box column configurations. In each series, the column had a plastic section modulus that was similar but higher than the beam such that it satisfied the strong column–weak beam criterion. The W36 column for the F series was included to investigate the effects of very deep columns, even though previous DFF testing with W36 columns had not indicated any torsional issues (Richards, 2021). The box column in the H-series investigated DFF configurations that do not require column cover plates [Figure 1(c)].

The details for each series are communicated in Figures 3 through 5. The H-series, with box columns, had a similar detail to the others, the only difference being that the box column did not require additional cover plates because the sides of the box column could function in that capacity (Figure 5).

Material Properties

The wide-flange beams and columns were ASTM A992 (ASTM, 2015b) steel while the plates and bars were ASTM A572 Gr. 50 (ASTM, 2015a). Material properties for the various steel components were determined from independent testing (American Metallurgical Services) as reported in Table 2.

Beam strength considerations were different for the DFF connections, as compared to other prequalified SMF connections, because the DFF beams were not designed to yield. From Table 2, some of the beam flanges had strength beyond $R_y F_y$ (Series E and G), while other were at $R_y F_y$ (Series F), or below $R_y F_y$ (Series H) (see Table 2). Because the fuse plates were proportioned to preclude beam yielding,

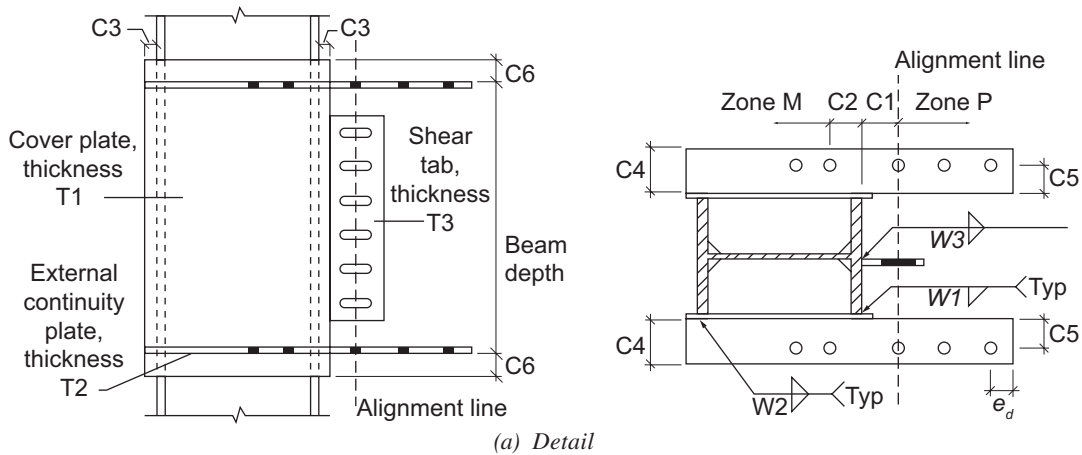
assuming a beam strength of only F_y , the same performance was expected regardless of beam strength beyond that.

Material for the fuse plates was selected to represent a conservative case from the standpoint of ductility and maximum force delivered to the connection. A572 Gr. 50 material with a high yield point was selected for the fuses because such material generally has lower toughness and ductility. The DFF design criteria prohibits the use of A572 Gr. 50 material with tensile strength greater than 85 ksi (UES, 2020). The fuse plates with relatively high strength (Table 2) also represented the critical case with regards to the maximum force that would be delivered to bolts, welds, and the other connection plates. Material for the other A572 Gr. 50 connection plates was intentionally selected to be as weak as could be acquired (Table 2) to represent a critical combination.

Fabrication

The plate components, including the fuse plates, were cut with a Kinetic K5200XMC plasma cutter. The specification for DFF states that “roughness of all thermal cut surface shall be no greater than an ANSI surface roughness of 1000 micro-in.” and “roughness exceeding this value or gouges not more than 3/16 in. shall be removed by machining and grinding.” However, to test poor fabrication of the fuse, gouges were introduced at the critical locations on each of the fuse plates and not ground smooth. The depth of the gouges was 1/8 in.

Bolt holes in the beams were drilled, while bolt holes in the external continuity plates, top plates, and fuse plates were either drilled or plasma cut. The method of bolt hole

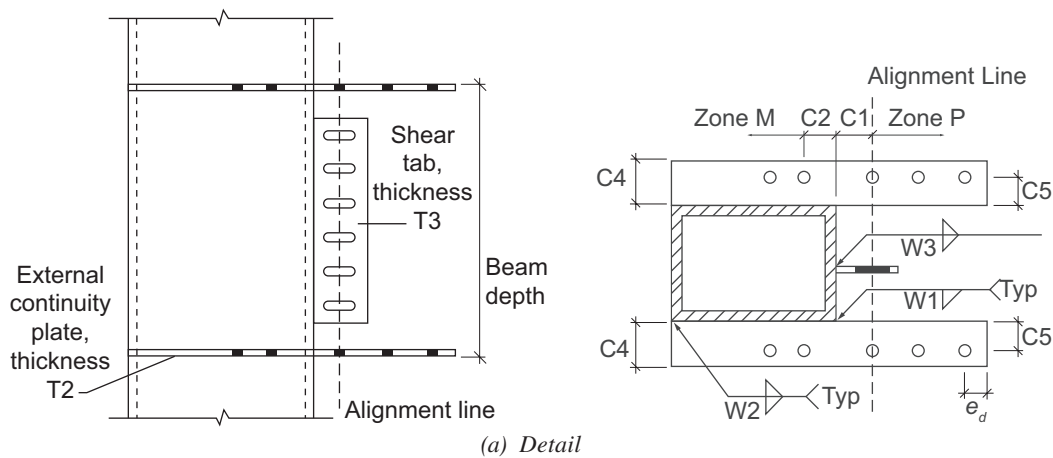


Specimens	Plate Thickness (in.)			Dimensions (in.)						Weld Sizes (in.)		
	T1	T2	T3	C1	C2	C3	C4	C5	C6	W1	W2	W3
E1.1 E1.2	0.625	0.75	0.5	3.75	5	1	4.75	3	3	9/16	3/8	3/8
F1.1 F1.2	0.875	1.25	0.625	4.75	1.25	1	5	3	3	5/8	3/8	7/16
G1.1 G1.2	0.375	0.625	0.5	2.875	1	1	3.5	2.313	3	7/16	1/4	5/16

Note: See Figure 5 for bolt quantities and spacing.

(b) Schedule

Fig. 3. Connection details for Series E, F, and G.

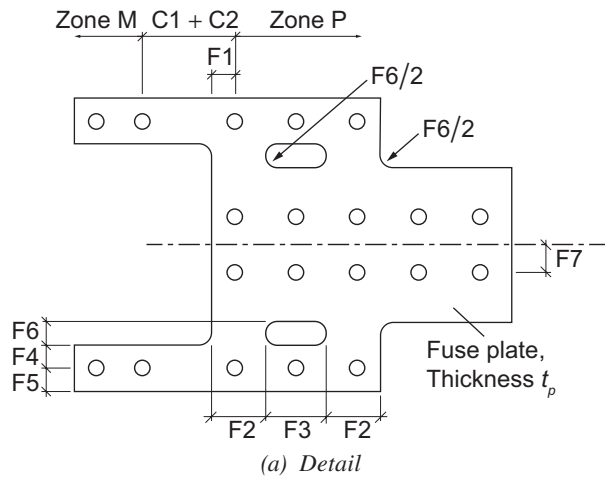


Specimens	Plate Thickness (in.)		Dimensions (in.)			Weld Sizes (in.)	
	T2	T3	C1 + C2	C4	C5	W2	W3
H1.1	1.75	0.875	3.75	5.25	3.5	3/4	1/2
H1.2 H1.3	1.75	0.875	3.75	6.125	3.5	1	1/2

Notes: See Figure 5 for bolt quantity and spacing.

(b) Schedule

Fig. 4. Connection details for Series H.



Specimen	Dimensions (in.)									Bolts	
	F1	F2	F3	F4	F5	F6	F7	C1 + C2	Bolt Spacing	P	M
E1.1	2	3.125	6.25	2	1.375	2.5	2.75	8.75	3	4	2
E1.2	2	3.375	5.75	2	1.375	3	2.75	8.75	3	4	2
F1.1	2	3.5	6.625	2.125	2	3.5	2.75	6	3.375	4	3
F1.2	2	3.6875	6.25	2.125	2	4	2.75	6	3.375	4	3
G1.1	1.5	1.875	4.5	1.375	1.1875	1.5	1.75	3.875	2.625	3	2
G1.2	1.5	1.875	4.5	1.375	1.1875	1.5	1.75	3.875	2.625	3	2
H1.1	2.25	3.3125	8.625	2.375	2.25	3	2.75	3.75	3.75	4	4
H1.2	2.25	3.3125	8.625	2.375	2.25	3	2.75	3.75	3.75	4	4
H1.3	2.25	3.5	8.25	2.375	2.25	4	2.75	3.75	3.75	4	4

(b) Schedule

Fig. 5. Fuse plate dimensions.

Table 2. Material Properties

Series	Component	Steel Grade	Yield Strength (ksi)	Tensile Strength (ksi)	Elongation (%)
E	Beam flange	A992	60.5	76	28
	Column flange	A992	52	78.5	28
	Fuse plate	A572 Gr. 50	58.3	84	29
	Cover plate	A572 Gr. 50	54	73.5	36.5
	Other plates	A572 Gr. 50	51.8	73.3	32.5
F	Beam flange	A992	55.5	74.5	33
	Column flange	A992	62	82	29
	Fuse plate	A572 Gr. 50	57.3	83.5	28
	Cover plate	A572 Gr. 50	(55) ^a	(77.8) ^a	(24) ^a
	Other plates	A572 Gr. 50	57.3	83.5	28
G	Beam flange	A992	60.5	78.5	33
	Column flange	A992	57	75.5	28
	Fuse plate	A572 Gr. 50	58	83.3	33.5
	Cover plate	A572 Gr. 50	59.3	75	33.5
	Other plates	A572 Gr. 50	54	73.5	36.5
H	Beam flange	A992	52.5	74	30
	Column flange	A992	52.5	79.8	29
	Fuse plate	A572 Gr. 50	54	83.3	28
	Cover plate	A572 Gr. 50	52.5	79.8	29
	Other plates	A572 Gr. 50	52.5	79.8	29

^a Values in parentheses were from mill reports; all others were determined from independent testing.

creation was not found to have any impact on test results.

All of the welds were produced in the shop in the flat position. The same electrode, Lincoln UltraCore 70C, AWS D1.8 (AWS, 2016) compliant, was used for all welds.

Bolting

A variety of bolt sizes, ASTM F3125 (ASTM, 2019) grades, and tightening methods were used. Bolts sizes ranged from 0.875 to 1.25 in. and are indicated in Table 1. Series E and F used Gr. F2280 bolts, Series G used Gr. F1852 bolts, and Series H used Gr. A490 bolts. For series E, F, and G, the bolts were pretensioned with a twist-off tool. For series H, the bolts were pretensioned using the turn-of-the-nut method. All of the bolt installations were performed in the laboratory. The grade of bolt, or bolt tightening method, was not found to have any impact on test results.

The E series investigated the impact of closing gaps with or without shims. For Specimen E1.1, there was a 3/16-in. gap between the west top plate and external continuity plates during loose fit-up. That gap was closed without shim plates during bolt tightening. For Specimen E1.2, similar gaps were present between the top plate and external continuity

plates and between the fuse plate and external continuity plates. Finger shims were used in the gaps prior to bolt tightening. The similar response of E1.1 and E1.2 indicated that finger shimming had negligible impact on behavior.

Loading Protocol and Instrumentation

The standard loading protocol specified in AISC 341, Section K2.4b (2016b), was used for all but one of the tests. The specified loading was six cycles at 0.00375-rad story drift, followed by six cycles at 0.005 rad, six cycles at 0.0075 rad, four cycles at 0.01 rad, two cycles at 0.015 rad, two cycles at 0.02 rad, two cycles at 0.03 rad, two cycles at 0.04 rad, and two additional cycles at each 0.01-rad increment up to failure. The actuator displacement corresponding to each drift level was calculated by multiplying the target rotation by the distance from the column centerline to the actuator line of action (see Figure 2).

For the first test in each series, the loading protocol was applied through the 0.04-rad drift cycles. Then, testing was stopped, the fuse plates (and bolts) were replaced, and another test was started. The last test in each series was continued all the way until fuse plate tearing occurred.

Conservative adjustments to the standard protocol were made at some points. For all the specimens tested with the standard protocol, the target displacement for the 0.04-rad cycles was increased from 0.001 to 0.003 rad to ensure that the inelastic rotation was at least 0.03 rad during those cycles. This was done because some qualification criteria are based on inelastic rotation rather than story drift. The other conservative deviations from the standard protocol occurred during F1.2 tests. During the first 0.05-rad cycle, an actuator control issue resulted in a larger-than-intended displacement of 0.068 rad.

Specimen H1.2 was the one specimen tested with a non-standard protocol. The protocol was developed by performing nonlinear response history analysis (RHA) on the moment frame in Section 4.3 of the *Seismic Design Manual* (AISC, 2018). RHA was performed using the 1994 Northridge (Beverly Hills–14145 Mulhol), 1989 Loma Prieta (Capitola), and 1995 Kobe (Shin-Osaka) records. The records were scaled to the maximum considered earthquake (MCE) level. The third-story drifts in the example building were the largest and were used for the protocol. The significant drift cycles from the Northridge, Loma Prieta, and Kobe responses were combined to form the protocol shown in Figure 6. The protocol has over 50 cycles and represents demands from three MCE events applied in sequence.

EXPERIMENTAL RESULTS

Observed Response

The observed response of Specimen E1.2 will be discussed in some detail because it was representative of the other specimens. Figure 7 shows photos of E1.2 at different stages of testing. The specimen appeared to remain elastic throughout the 0.00375-, 0.005-, 0.0075-rad cycles. During the 0.01-rad cycles, slight flaking of the mill scale indicated localized yielding in the yield regions [Figure 7(a)]. Bolt slip occurred during the 0.015-rad and subsequent cycles. During the 0.02-, 0.03-, and 0.04-rad cycles, inelastic

deformations of the fuse plate became more pronounced [Figure 7(c)–(e)]. The external continuity plates had noticeable curvature at 0.05-rad drift [Figure 7(f)] but were still primarily elastic (the plates were essentially straight after testing). During the second cycle at 0.06 rad, ductile tearing of the fuse plate initiated [Figure 7(g)], and during the first excursion to 0.07 rad, the west side of the fuse plate tore through [Figure 7(h)].

The other specimens had similar observed response, with localized yielding occurring around 0.01 rad, followed by bolt slip, significant fuse plate yielding (for drifts beyond 0.02 rad), and eventually fuse plate tearing. Figure 8 shows photos from each series at 0.05 rad.

Table 3 summarizes the cycles that were completed by each specimen. The first specimen in each series was only tested to 0.04 rad so that the fuse plates could be replaced to demonstrate repairability. Specimens E1.2, G1.2, and H1.3 all completed cycles at 0.06 rad. Specimen F1.2 completed two cycles at 0.05 rad; however, one of them included an unintended excursion to 0.068 rad. In general, the cyclic rotation capacity was greater for the shallower beams because the strains in the fuse plates were proportional to the beam depth.

While incidental yielding was observed in various elements, significant inelastic deformations were confined to the fuse plates. Minor yielding of the reentrant corner of the top plates occurred for all the specimens (Reynolds and Uang, 2019a), but the top plates did not require replacement. The same top plates were used for multiple tests in Series F, G, and H. For the F series, minor flaking of the mill scale was observed in the proximity of the beam flange bolt holes and in the shear tab plate. Overall, however, the beams, columns, and panel zones remained essentially elastic throughout testing (Figure 8).

Specimen H1.2 was tested with a nonstandard protocol. The customized protocol reflected demands from three MCE events applied in sequence. Specimen H1.2 exhibited fuse yielding and bolt slip during testing, but no tearing in the fuse, and no significant yielding in other components.

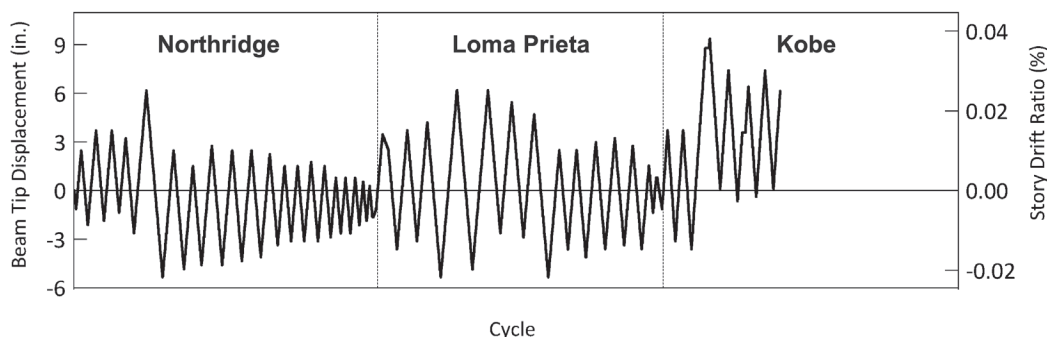
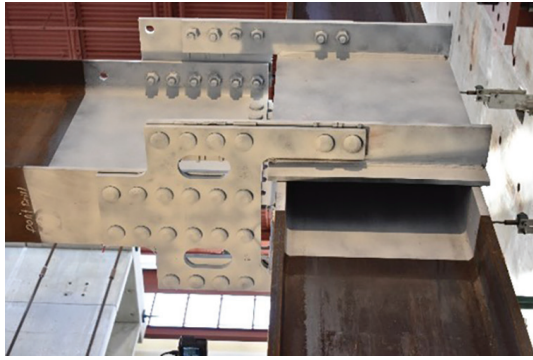


Fig. 6. Nonstandard protocol representing three MCE events applied sequentially.



(a) 0.01 rad



(b) 0.015 rad



(c) 0.02 rad



(d) 0.03 rad



(e) 0.04 rad



(f) 0.05 rad



(g) 0.06 rad

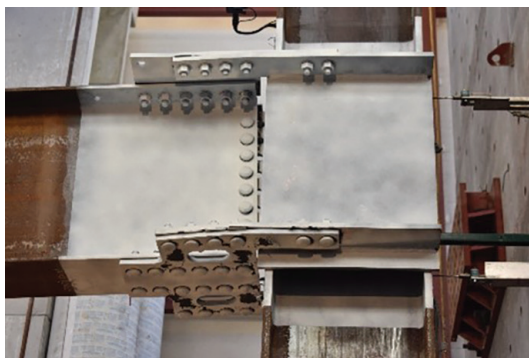


(h) 0.07 rad

Fig. 7. Connection behavior at various cycles of loading, EI.2 shown.

Table 3. Cycles Completed and Maximum Applied Force for Each Specimen			
Specimen	Beam	Cycles Completed [rad (number of cycles)]	Maximum Actuator Force (kips)
E1.1	W30×99	0.04 (2) ^a	80.8
E1.2		0.06 (2)	91.8
F1.1	W40×167	0.04 (2) ^a	206
F1.2		0.05 (2) ^b	225
G1.1	W21×50	0.04 (1) ^a	30.3
G1.2		0.06 (2)	33.5
H1.1	W36×232	0.04 (2)	179
H1.2		— ^c	177
H1.3		0.06 (1)	225

^a The first test in each series was stopped after 0.04 rad so that the fuse plate could be replaced to demonstrate reparability.
^b Due to an actuator control problem, F1.2 was pushed to 0.068 rad during the first 0.05-rad cycle.
^c Specimen H1.2 was tested with a nonstandard protocol with unsymmetric cycles.



(a) E1.2



(b) F1.2



(c) G1.2



(d) H1.3

Fig. 8. Specimens from each series at 0.05 rad.

Measured Response

The hysteretic behavior of the DFF connections is shown in Figure 9, where the moment at the column face is plotted versus the story drift for each of the specimens. The moment at the column face was calculated as the actuator load multiplied by the distance from the actuator line of action to the column face. The moment at the column face was normalized by the nominal plastic moment of the beam, M_{pn} , on the right side of each plot. Horizontal dashed lines were added at $0.8M_p$, which is the strength degradation threshold when determining rotation capacity (AISC, 2016b). The drift was calculated as the displacement at the actuator line of action divided by the distance from the actuator line of action to the centerline of the column. Vertical dashed lines were added to the plots at 0.04-rad drift, which is the qualification criteria for special moment frames (AISC, 2016b).

Hysteretic response of the DFF connections was similar to other bolted SMF connections, except there was no strength degradation at large drifts. As with other bolted SMF connections (Sato et al., 2008), the DFF hysteretic plots had a flatter region in the middle of each large cycle corresponding to bolt slip (Figure 9). Once bolts returned to bearing, the strength continued to climb. One difference, as compared to other bolted SMF connections, was the lack of strength degradation at large drifts. SMF connections that form plastic hinges in the beam have strength degradation after 0.03 or 0.04 rad due to flange and web local buckling of the beam in the plastic hinge region (Uang and Fan, 2001). The DFF connections did not have flange local buckling or local buckling in the fuse plate, and maintained strength through large drift cycles until the fuse plates fatigued.

The hysteretic response of H1.2 (Figure 10) was consistent with H1.1 and H1.3 tested with the standard protocol. The nonsymmetric hysteretic plot for H1.2 would fit within the envelopes of the H1.1 or H1.3 responses [comparing Figure 10 with Figure 9(g), (h)].

Connection Stiffness

Experimental results were used to quantify the stiffness of the DFF connections. During testing, the actuator force, F , and beam displacement, δ , were recorded. For the elastic cycles, the beam displacement was the sum of the displacement effects caused by beam deformations, δ_b , column deformations, δ_c , panel zone deformations, δ_{pz} , and connection deformations, δ_{con} .

$$\delta = \delta_b + \delta_c + \delta_{pz} + \delta_{con} \quad (1)$$

Displacement effects from connection deformations, δ_{con} , were determined by subtracting beam, column, and panel zone displacement effects from the total measured displacement (rearranging Equation 1). The total deformation was taken from the first peak at 0.00375 rad. Beam and

column deformation effects, δ_b and δ_c , were determined using Timoshenko beam theory and the measured applied force on the beam, F , and the calculated reaction forces on the column. Panel zone deformation effects, δ_{pz} , were computed by multiplying the measured panel zone shear deformation by the distance from the column face to the actuator. With δ , δ_b , δ_c , and δ_{pz} all known, δ_{con} was calculated from Equation 1. Table 4 summarizes values of δ , δ_b , δ_c , δ_{pz} , and δ_{con} from the initial 0.00375-rad cycle for the first test in each series.

An effective spring stiffness was calculated for the connections as:

$$K_s = \frac{M}{\theta} = \frac{Fg}{\left(\frac{\delta_{con}}{g}\right)} \quad (2)$$

where g was the distance from the actuator line of action to the face of the column. Calculated values for K_s are summarized in Table 5.

Moment frame connections are considered fully restrained (FR) for design purposes if the connection stiffness is large relative to the flexural stiffness (EI/L) of the beam. In AISC 358, *Prequalified Connections for Special and Intermediate Steel Moment Frames for Seismic Applications*, Chapter 13 Commentary (2016a), a minimum stiffness of $18EI/L$ is discussed. In AISC 360, *Specification for Structural Steel Buildings*, Section B3 Commentary (2016c), $20EI/L$ is discussed as a level of acceptability. Relative to these specifications, the normalized values of K_s shown in the last column of Table 5 were sufficient to classify the DFF connection as FR.

SUMMARY AND CONCLUSIONS

Connections in steel special moment frames (SMF) must be capable of accommodating large story drifts without excessive strength deterioration. Most SMF connections rely on beam yielding to achieve large inelastic rotations. In contrast, DuraFuse Frames (DFF) moment connections are designed so that yielding occurs in a fuse plate, making DFF SMF easier to repair after severe earthquakes. As part of the prequalification for DFF connections, full-scale testing was conducted in accordance with AISC 341, Chapter K. Nine specimens were tested at UCSD, with beam sizes of W21×50, W30×99, W36×232, and W40×167.

The experiment results support the following conclusions:

- The eight specimens that were tested with the standard protocol all met the AISC 341 acceptance criteria by completing at least one cycle at 0.04 rad without strength degradation below $0.8M_{pn}$.
- The series with W21×50 and W30×99 beams completed two cycles at 0.06 rad prior to fuse tearing. The heaviest

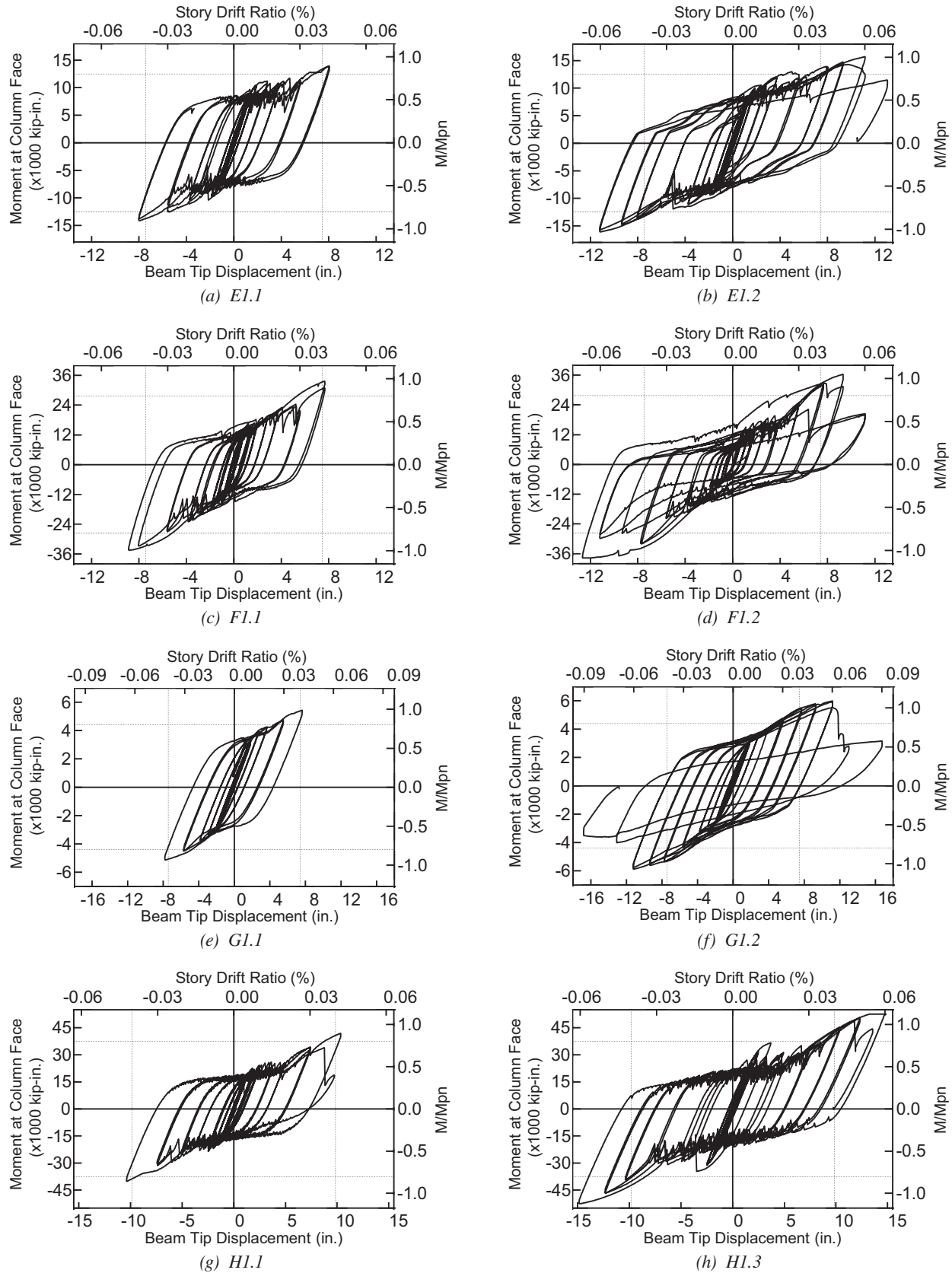


Fig. 9. Hysteretic response for the DFF specimens tested with standard protocol.

Specimen	F (kips)	δ (in.)	δ_b (in.)	δ_c (in.)	δ_{pz} (in.)	δ_{con} (in.)
E1.1	28.7	0.726	0.477	0.132	0.0797	0.0387
F1.1	36.1	0.312	0.191	0.0398	0.0671	0.0137
G1.1	10.0	1.07	0.694	0.214	0.0805	0.0810
H1.1	55.0	0.865	0.581	0.123	0.0751	0.0852

Specimen	Beam	I (in. ⁴)	L^a (in.)	$\frac{EI}{L}$ (kip-in.)	K_s (kip-in./rad)	$\frac{K_s}{EI/L}$
E1.1	W30×99	3,990	372	311,000	22,700,000	73
F1.1	W40×167	11,600	372	904,000	74,000,000	82
G1.1	W21×50	984	372	76,700	3,960,000	52
H1.1	W36×232	15,000	492	884,000	35,400,000	40

^a Bay width of the prototype frame.

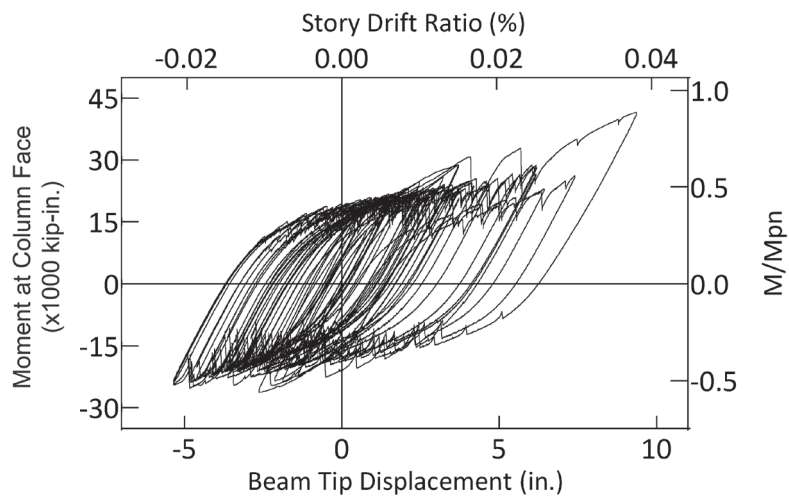


Fig. 10. Hysteretic response of H1.2, tested with alternative loading protocol.

series, with a W36×232 beam, completed one cycle at 0.06 rad prior to fuse tearing.

- Testing under an earthquake-specific protocol demonstrated that DFF fuse plates can withstand multiple MCE events in sequence without requiring replacement.
- DFF connections were found to be fully restrained (FR) with the experimentally determined connection stiffness exceeding $20EI/L$ for the full range of sizes.
- DFF connections did not experience strength degradation at large drifts since beam local buckling was prevented. Fuse plates maintained their strength until ductile tearing occurred.
- DFF connections were repaired by replacing the bottom fuse plate. Repeatable performance was demonstrated after fuse plates were replaced. Fuse yielding for drifts up to 0.02 rad was localized and would not necessitate fuse replacement.

ACKNOWLEDGMENTS

This work was funded by DuraFuse Frames LLC in West Jordan, Utah. Experimental testing was conducted at the University of California–San Diego (UCSD). The primary UCSD personnel involved with the project were Mathew Reynolds, Professor Chia-Ming Uang, Dr. Christopher Latham, and Andrew Sanders. Chao-Hsien Li performed the nonlinear response history analyses that were the basis for the alternative loading protocol. The work of these individuals is gratefully acknowledged.

The DFF connection is proprietary, but licenses for use are granted on reasonable and nondiscriminatory terms.

REFERENCES

- AISC (2016a), *Prequalified Connections for Special and Intermediate Steel Moment Frames for Seismic Applications*, ANSI/AISC 358-16, American Institute of Steel Construction, Chicago, Ill.
- AISC (2016b), *Seismic Provisions for Structural Steel Buildings*, ANSI/AISC 341-16, American Institute of Steel Construction, Chicago, Ill.
- AISC (2016c), *Specification for Structural Steel Buildings*, ANSI/AISC 360-16, American Institute of Steel Construction, Chicago, Ill.
- AISC (2018), *Seismic Design Manual*, 3rd Ed., American Institute of Steel Construction, Chicago, Ill.
- ASCE (2016), *Minimum Design Loads and Associated Criteria for Buildings Structures*, ASCE/SEI 7-16, American Society of Civil Engineers, Reston, Va.
- ASTM (2015a), *Standard Specification for High-Strength Low-Alloy Columbium-Vanadium Structural Steel*, A572/A572M, ASTM International, West Conshohocken, Pa.
- ASTM (2015b), *Standard Specification for Structural Steel Shapes*, A992/A992M, ASTM International, West Conshohocken, Pa.
- ASTM (2019), *Standard Specification for High-Strength Structural Bolts and Assemblies, Steel and Alloy Steel, Heat Treated, 120 ksi (830 MPa) and 150 ksi (1040 MPa) Minimum Tensile Strength, Inch and Metric Dimensions*, F3125/F3125M, ASTM International, West Conshohocken, Pa.
- AWS (2016), *Structural Welding Code—Seismic Supplement*, D1.8/D1.8M, American Welding Society, Miami, Fla.
- Reynolds, M. and Uang, C.-M. (2019a), *Cyclic Testing of DuraFuse (DF) Moment Frame Connections for SMF and IMF Applications: Series E, F, and G Specimens*, TR19-01, University of California San Diego, La Jolla, Calif.
- Reynolds, M. and Uang, C.-M. (2019b), *Cyclic Testing of DuraFuse (DF) Moment Frame Connections for SMF and IMF Applications: Series H Specimens*, TR19-02, University of California San Diego, La Jolla, Calif.
- Richards, P.W. (2019), “A Repairable Connection for Earthquake-Resisting Moment Frames,” *Steel Construction*, Vol. 12, No. 3, pp. 191–197.
- Richards, P.W. (2021), “Cyclic Hardening Factor for Replaceable Shear Fuse Connections,” *Journal of Constructional Steel Research*, Vol. 185, 106838.
- Richards, P.W. and Oh, S.S. (2019), “Cyclic Behavior of Replaceable Shear Fuse Connections for Steel Moment Frames,” *Journal of Structural Engineering*, Vol. 145, No. 12, 04019156.
- Sato, A., D. Newell, J., and Uang, C.-M. (2008), “Cyclic Behavior and Seismic Design of Bolted Flange Plate Steel Moment Connections,” *Engineering Journal*, AISC, Vol. 45, pp. 221–232.
- Uang, C. and Fan, C. (2001), “Cyclic Stability Criteria for Steel Moment Connections with Reduced Beam Section,” *Journal of Structural Engineering*, Vol. 127, No. 9, pp. 1021–1027.
- UES (2020), *DuraFuse Frames Technology*, UES ER-610, IAPMO Uniform Evaluation Services, Ontario, Calif.